ADVANCED ELECTRONIC MATERIALS
Open Access
www.advelectronicmat.de

Toward Highly Efficient Solution-Processable OLEDs: Inkjet Printing of TADF Emissive Layer

Marco Cinquino, Carmela Tania Prontera, Antonio Maggiore, Alessandra Zizzari, Marco Pugliese, Fabrizio Mariano,* Vitantonio Valenzano, Ilaria Elena Palamà, Riccardo Manfredi, Giuseppe Gigli, and Vincenzo Maiorano*

The fabrication of optoelectronic devices using low-cost inkjet printing techniques is a topic of great interest to the scientific and industrial community and represents a step toward the full deployment of solution-processable organic light emitting diodes (OLEDs), particularly for commercial lighting and signaling applications. Herein, the inkjet printing of tBuCzDBA (9,10-bis(4-(3,6-di-*tert*-butyl-9*H*-carbazol-9-yl)−2,6-dimethylphenyl)−9,10-diboraanthracene) is reported, a high-performing thermally activated delayed fluorescence (TADF) emitter for OLEDs. Optimizing the surface tension values of the ink formulations and the associated wetting behavior are crucial parameters for achieving a uniform and homogeneous printed thin film. In particular, it is observed that using a proper mixture of solvents with different surface tensions, it is possible to generate Marangoni flows inside the drop, which triggers a very fast drying process, ensuring optimized morphological and optical properties in the inkjet printed tBuCzDBA-based film. OLEDs exploiting this film as an emissive layer are then fabricated, achieving a maximum luminance of 32 000 cd m^{-2}, a current efficiency of 27.5 cd A^{-1}, and an external quantum efficiencyof 10%. To the best of the knowledge, this is the highest efficiency reported to date for self-hosted TADF inkjet-printed OLEDs.

1. Introduction

Organic electronics is a dominant area of technological research, contributing to our everyday lives with a steady stream of new applications. These include OLEDs, a type of thin-film light-emitting electronic device that converts electrical energy into light. These devices have attracted exceptional attention in the organic electronics context due to their outstanding advantages over conventional lighting and display technologies. In particular, OLEDs offer high luminous efficiency, low power consumption, wide viewing angle, cost advantages, lightweight, flexibility, and solution-based processability.[1–7] OLED devices consist of several layers of organic materials sandwiched between two conducting electrodes. The deposition process is critical for OLEDs performances as it affects the quality, thickness, and uniformity of the films. The most common deposition technique for OLEDs is thermal evaporation, a process needing a vacuum chamber, which allows for the best device performance in terms of luminance and efficiency. However, the sublimation suffers from the drawback of being a high-cost and low-scalable process.[8–11] Film-forming technologies based on solution processes are increasingly being used as a simple, fast, and cost-effective alternative to thermal evaporation. Such processes can be divided into coating and printing techniques. Spin coating,[12,13] dip coating,[14] blade coating,[15] and spray coating[16] belong to the first category, and are widely used to obtain high-quality thin films in a simple and low-cost way. Unfortunately, these techniques are not always suitable for large-scale deposition, suffer from high material waste and don't allow for defined geometric deposition.[17–19] Alternatively, printing techniques allow high throughput deposition of thin films with a two-dimensional pattern and reduced material consumption.[20–23]

In particular, inkjet printing is one of the most exciting printing techniques, based on the propulsion of droplets of specially designed ink onto a substrate, to create a digital image. Such a technique has several advantages, such as high resolution and high-speed deposition with minimal material waste,[24,25]

M. Cinquino, G. Gigli
Department of Mathematics and Physics
University of Salento
via Monteroni, Lecce 73100, Italy

M. Cinquino, C. T. Prontera, A. Maggiore, A. Zizzari, M. Pugliese, F. Mariano, V. Valenzano, I. E. Palamà, R. Manfredi, G. Gigli, V. Maiorano
CNR-NANOTEC – Institute of Nanotechnology
c/o Campus Ecotekne, Via Monteroni, Lecce 73100, Italy
E-mail: marco.pugliese@nanotec.cnr.it;
fabrizio_mariano@klopman.com

M. Pugliese, F. Mariano
Klopman Internationl Srl
Via Armando Vona 34, Frosinone 03100, Italy

The ORCID identification number(s) for the author(s) of this article can be found under https://doi.org/10.1002/aelm.202300358

DOI: 10.1002/aelm.202300358

Table 1. Physical properties of solvents and inks employed.

Ink	Solvents	Density [g mL^{-1}]	Boiling Point [°C]	Surface tension [mN m^{-1}]	Viscosity [mPa s]
	Toluene*	0.865	110	28.4	0.59
	Chloroform*	1.492	61	27.5	0.58
	O-dichlorobenzene*	1.306	180	36.6	1.32
T#1	Toluene (tBuCzDBA 0.25 mg mL^{-1})	0.794	≈110	30.1 ± 0.9	0.66 at 100 s^{-1}
T#2	Toluene/chloroform 1/29 vol. ratio (tBuCzDBA 0.25 mg mL^{-1})	1.316	≈61	21.9 ± 0.2	0.64 at 100 s^{-1}
T#3	Toluene /chloroform /o-dichlorobenzene 1/28/1 vol. ratio (tBuCzDBA 0.25 mg mL^{-1})	1.351	≈61	25.5 ± 0.7	0.91 at 100 s^{-1}

*From Yaw's Handbook of Thermodynamic and Physical Properties

compatibility with different substrates, and high pattern precision without the need to use masks during deposition.[25–28] This last aspect is particularly promising for the deposition of multilayer structures without the need for masks and/or complex patterning techniques.[29] Despite the potentiality of inkjet printing, there is still much progress to be made before it can be fully applied to organic electronics and OLEDs fabrication.

The emissive layer deposition is one of the most critical part in inkjet printed OLED devices and among the emitters commonly used in OLEDs, TADF materials have recently been investigated and used with increasing interest in both academic and industrial research for the fabrication of high-performance devices. In particular, TADF is a mechanism by which some organic molecules can emit light by delayed fluorescence, achieved by converting triplet excitons back to singlet with high efficiency. They have achieved significant success because they are fully organic materials that allow the harvesting of dark triplet excitons under electroluminescence, thus obtaining 100% IQE without using traditional phosphorescent organometallic complexes, which are expensive, toxic, and rare.[30] TADF materials are organic small molecules,[31–35] polymers,[36–39] and dendrimers[40–42] characterized by the presence of almost isoenergetic triplet and singlet electronic excited states. This key feature allows the up-conversion of triplets into singlets through the reverse intersystem crossing (RISC) process, activated by thermal energy[43] and mediated by second-order vibronic coupling.[44]

Amruth et al.[45] developed a new TADF based on a triazine core carbazole dendrimer with tert-butyl side groups, which exhibited high solubility in organic solvents, and it was inkjet printed from a toluene/tetralin mixture. The resulting OLED device achieved a current efficiency of 18 cd A^{-1} and a maximum luminance of 6700 cd m^{-2}. Another interesting result was obtained by Cole et al.[46] who reported a solution-processable TADF polymer as a self-hosted inkjet printed emitting layer in OLEDs, achieving a current efficiency of ≈5 cd A^{-1}. In this context, we report the inkjet printing of tBuCzDBA as TADF-based emitting layer in OLED devices. The first OLED with tBuCzDBA was published in 2018[47] and it was based on a thermal evaporated host-guest system. Afterward, it has been used as guest material in a host-guest systems deposited by spin coating, achieving very high EQEs.[48,49] Moreover, Wu et al.[50] have shown that pure tBuCzDBA can be successfully used as non-doped emitting material in OLED thanks to the tert-butyl groups, which can reduce the degree of aggregation and thus the self-quenching. Therefore, here we report the inkjet printing of thin film of pure tBuCzDBA as an application in self-hosted TADF-based devices as an easy approach for solution-processable OLEDs. To the best of our knowledge, this material has never been deposited using inkjet printing, and therefore, due to its excellent optoelectronic characteristics, we have developed a suitable ink to achieve good thin film properties allowing for high device performance.

2. Results and Discussion

2.1. Ink Optimization

The first step in optimizing an inkjet printing process is to develop the right ink formulation. The ink must meet at least two basic requirements, at the same time: firstly, it must not completely re-dissolve other underlying organic layers; secondly, it must have adequate physical properties to ensure a uniform printed film.

To optimize the ink, we started from a toluene-only formulation, evaluating its characteristics and printability. Subsequently, we selected and added other solvents (chloroform and o-dichlorobenzene) with the aim of improving the quality of the printed film. This resulted in three ink formulations containing tBuCzDBA, the properties of which are shown in **Table 1** together with those of their base components.

The first ink (T#1) was based on a 0.25 mg mL^{-1} solution of tBuCzDBA in toluene and was characterized by a surface tension of 30.1 ± 0.9 mN m^{-1} and a viscosity of 0.66 mPa s at 100 s^{-1} (Table 1, and black line in Figure S1, Supporting Information). A glass/poly(9-vinylcarbazole) (PVK – $M_w \approx 1.100.000$) substrate was used to study the wetting behavior associated with the three inks, as PVK was selected as the electron blocking layer in the OLED structure. The contact angle of T#1 on a glass/PVK substrate was studied over time and the results are shown in **Figure 1**a.

A single drop of T#1 deposited on PVK at $t_0 = 0$ s showed a low contact angle (7.8° ± 0.7°) which decreased to 2.8° ± 0.6° after 30 s, while the contact line remained almost unchanged. After 50 s the contact angle dropped to zero and the contact line receded by ≈20% from its initial position (at t_0). After 55 s almost complete drying was visible. As shown in Figure 1d, the final result was a drop characterized by a strong coffee-ring effect and a not homogeneous pattern in which tBuCzDBA is mainly

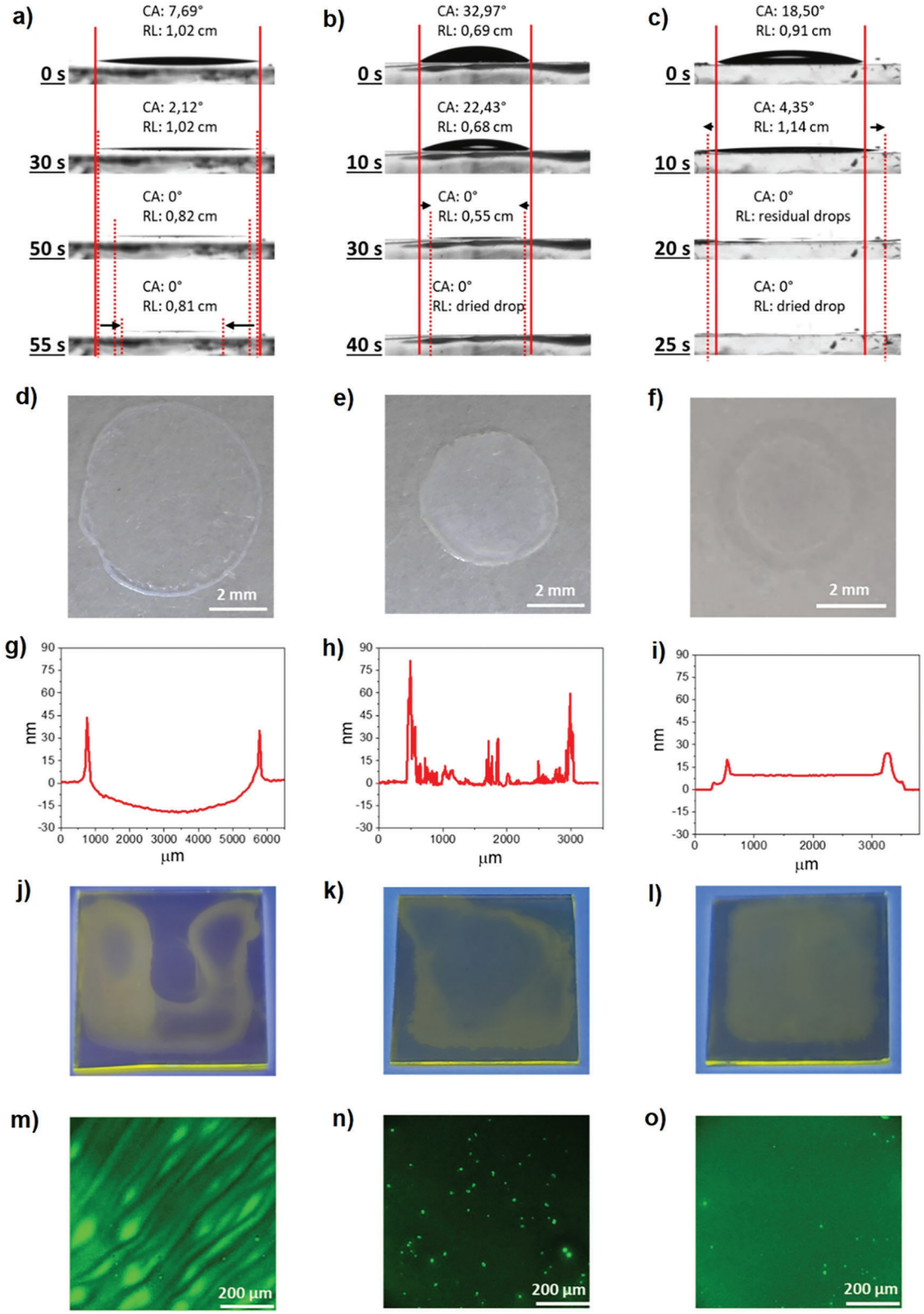

Figure 1. (Columns from left to right) T#1, T#2, T#3 ink formulations characteristics. a–c) Sessile drop contact angle measurement versus time of single drop of T#1, T#2, and T#3 inks, respectively; the drops have been deposited on a PVK thin film, in order to reproduce the manufacturing conditions of the OLED device; the contact angle decreases over time and the edges of the drops move inwards or outwards depending on the ink formulation. d–f) images of single dry drop of T#1, T#2, and T#3 inks under optical microscope (Dino-Lite); g–i) T#1, T#2, and T#3 dry drops profile, deposited on a PVK thin film; j–l) inkjet printed dry film under UV radiation: inks formulation significantly affects the film morphology; m–o) confocal laser scanning

localized in concentric circles on the the drop edge, as also confirmed by confocal fluorescence images reported in Figure S2a (Supporting Information). The drop profile is shown in Figure 1g and confirms the strong coffee ring effect together with a reduction in the total film thickness in the central area of the drop, presumably due to the redissolution of the underlying PVK. As a result, despite the high wettability, T#1 did not provide a uniform dry film. Indeed, the high boiling point of T#1 causes a slow drying process, resulting in a dewetting effect in which the contact line of the drop moves inward instead of pinning up on the substrate, resulting in a discontinuous thin film deposition.[51,52] In addition, the selected solvent dissolve the underlying layer and this effect is emphasized by the slow drying process. This is one of the most common problems in printing and/or solution-based deposition of multilayer structures. To further test T#1, an inkjet printed film with a square pattern of ≈3 cm^2 was deposited. The obtained printed film (observed under a UV lamp) is quite uneven thus showing that, during the slow drying process, the printed drops moved and rearranged on the substrate, thus not maintaining the pattern (a square) of the printing process (Figure 1j). The same sample was also observed under a confocal laser scanning microscope, showing no fluorescence from the centre of the sample, while an intense but non-uniform fluorescence was visible at the edge of the printed region (Figure 1m), generated by the dewetting-induced material accumulation. This behavior confirms that the printed droplets migrate toward the edge of the sample and do not allow a uniform deposition. To improve the quality of the deposition, the possibility of accelerating the drying time by using a low boiling point cosolvent was then investigated.[52]

Chloroform was chosen as cosolvent for T#2 ink formulation because of its excellent solubilizing capacity for tBuCzDBA and its low boiling point (61.2 °C) compared to toluene. In particular, T#2 was based on a toluene/chloroform mixture having 1/29 volume ratio, using chloroform to speed up the drying process, while retaining a small amount of toluene to avoid too fast evaporation at the nozzle-air interface, which could cause nozzle clogging. In particular, T#2 was prepared by using the minimum part of toluene that did not produce a relevant dewetting effect. T#2 ink was characterized by a surface tension of 21.9 ± 0.2 mN m^{-1} and a viscosity of 0.64 mPa s at 100 s^{-1} (Table 1; Figure S1, Supporting Information, red line). The single T#2 drop deposited on PVK showed an initial contact angle of 31.2° ± 2.3° that dropped to 21.3° ± 2.5° after 10 s with the contact line that remained pinned to the substrate (Figure 1b). After 30 s, a contact line recession of ≈20% from initial position and a drastic contact angle reduction were visible. The drop was completely dried after 40 s. Such behavior demonstrated that the presence of chloroform reduced the wettability capacity of the ink but at the same time lowered the boiling point of the ink and, as a consequence, reduced the drying time. Despite the reduction in the drying time and dewetting effect, the final dry drop showed still a significant coffee ring effect and a very rough surface as evidenced by the drop profile reported in Figure 1h. The opaque appearance of the drop (Figure 1e) confirms the high roughness, which could also negatively affect the photoluminescence (see also Figure S2b, Supporting Information). The printed thin film observed under UV light still showed significant dewetting, which did not allow uniform deposition (Figure 1k). In addition, the presence of aggregates and a quenching of the photoluminescence were visible by observing the printed sample under a confocal laser scanning microscope (Figure 1n). The alternation of dark areas and bright spots indicated that tBuCzDBA tended to thicken during the drying rather than being evenly distributed. As a result, the reduction in drying time and dewetting, achieved by the addition of chloroform, was still not sufficient to obtain a uniform dry layer of the emissive material.

To improve the quality of the inkjet-printed film, a third solvent was added to the ink formulation. O-dichlorobenzene was chosen as the cosolvent with a high boiling point (180 °C) and high surface tension (37 mN m^{-1}). The T#3 ink consisted of a solvent mixture of toluene/chloroform/o-dichlorobenzene in a volume ratio of 1/28/1, respectively. T#3 showed a surface tension of 25.5 ± 0.7 mN m^{-1} and a viscosity of 0.91 mPa s at 100 s^{-1} (Table 1; Figure S1, Supporting Information, blue line). The single drop of T#3 deposited on PVK showed an initial contact angle of 18.9° ± 0.7° (Figure 1c), which is an intermediate value compared to the T#1 and T#2 formulations, as in the case of surface tension. For T#3, a drop propagation was evident, with an increase in the contact line of ≈20–25% from the position at t_0 and a reduction in the contact angle to 4.6° ± 0.6° after 10 s; after 20–25 s the drop was completely dry (Figure 1c). As can be seen in the supporting video (Video S3, Supporting Information), after the initial spreading, solution recirculation flows were visible inside the drop, causing almost instantaneous and uniform drying (videos of the other two formulations are also shown for comparison). Such behavior can be imputed to the Marangoni effect caused by the higher surface tension of o-dichlorobenzene (37 mN m^{-1}) compared to the other two solvents (26 mN m^{-1} and 27.4 mN m^{-1} for chloroform and toluene, respectively). Since a liquid with a high surface tension pulls on the surrounding liquid more strongly than one with a low surface tension, the presence of a surface tension gradient will naturally cause the liquid to flow away from regions of low surface tension.[53] In this case, the addition of o-dichlorobenzene created a surface tension gradient and consequently, a liquid flow that flattened the drop, reducing the drying time despite the higher boiling point. The final result was a glossy, dry drop with a uniform thickness and a coffee ring that was significantly reduced compared to the previous two inks (Figure 1f,i; Figure S2c, Supporting Information). Such an effect was also visible on the inkjet printed film, as shown by the picture of the printed film under a UV lamp and the confocal microscope images (Figure 1l,o). The printed thin film obtained with T#3 retained the print pattern and dried evenly without the formation of holes (Figure 1l). Despite the good quality of the film obtained with this formulation, redissolution of the underlying PVK cannot be completely excluded, given the nature of the solvents used. This aspect could have an important impact on the

microscopy images of inkjet printed films, highlighting the photoluminescence of tBuCzDBA; for ink T#2 n) and T#3 o), the images refer to the central region of the film, while for T#1 m) the image refers to the left part of the film shown in (j), because in this case the central region has no material deposited on it.

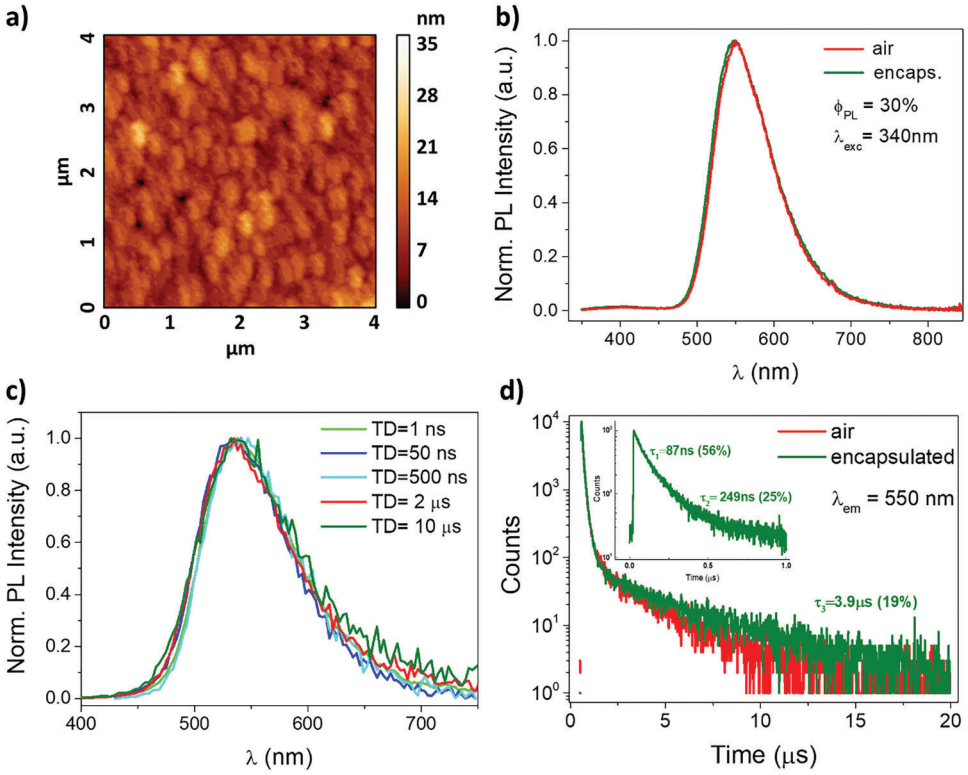

Figure 2. a) AFM image of inkjet printed tBuCzDBA thin film, b) normalized steady-state PL spectra of inkjet printed tBuCzDBA thin film, c) time-resolved emission spectra of the inkjet printed tBuCzDBA thin film, d) photoluminescence decay of tBuCzDBA thin film in the microsecond scale (inset: decay in the nanosecond scale). λex = 405 nm.

characteristics of the printed film and the device and therefore needs to be investigated. We measured the photoluminescence (PL) spectrum of the spin-coated PVK layer before and after various solvent treatments. In particular, we prepared the solvent mixture employed in T#3 (without tBuCzDBA) and printed and spin-coated such a mixture on top of the spin-coated PVK. The results are shown in Figure S3 (Supporting Information). As can be seen, when such a mixture is printed on top of the PVK layer, the emission peak is reduced by about half, whereas when such a mixture is spin-coated, the emission is strongly affected (≈90% of PL reduction). Such spectra show that the solvent mixture used for the printing (T#3) can dissolve the PVK layer and that this effect is more intense in the case of spin-coating. When print with such a solvent mixture, although there is no centrifugal force to wash out the material, a minimal coffee ring effect after drying can thin the PVK layer (as suggested by the reduction of the PL peak intensity). We also measured the PL of the PVK layer after spin-coating with toluene as a reference solvent for the spin-coating of the active layer and we observed a reduction in the PL peak intensity comparable to that observed when printing with the T#3 solvent mixture. Considering such a trend, we can assume that in both cases (printing with T#3 solvent mixture and spin-coating with toluene) a comparable reduction in the thickness of the PVK is achieved. The effect of the redissolution phenomena on the device performance will be discussed in detail in Section 2.3.

Based on the obtained results, a morphological and photophysical characterization was carried out on the film printed with the T#3 ink formulation, to evaluate its use as an active layer of an OLED device.

2.2. Morphological and Photophysical Characterization

One of the most critical question of OLEDs manufacturing is the thin film morphology. Therefore, the surface of the inkjet printed tBuCzDBA film was evaluated by atomic force microscopy (AFM). A representative AFM image of the printed thin film is shown in **Figure 2**a, which shows a granular morphology with a grain size in the order of hundreds of nanometres and a uniform surface with very low roughness (RMS – root mean square = 3.17 nm), which confirms the film uniformity and its suitability for OLED devices.

In addition, the photophysical properties of the presented printed film were studied. Steady-state photoluminescence spectrum is shown in Figure 2b with the corresponding photoluminescence quantum yeld (PLQY) value. Figure 2c shows the time-resolved PL spectra of the film, which provide insight into the nature of the states involved in the prompt and delayed emission. We can see that the PL emission remains the same regardless of the time delay (TD), ranging from 1n to 10 µs, thus indicating that the emission originates from the same singlet state. This demonstrates that the observed delayed emission is due to the population of the triplet state which is up-converted back to the singlet by RISC (TADF). The luminescence decay traces are shown in Figure 2d. We observe two monoexponential decay regimes:

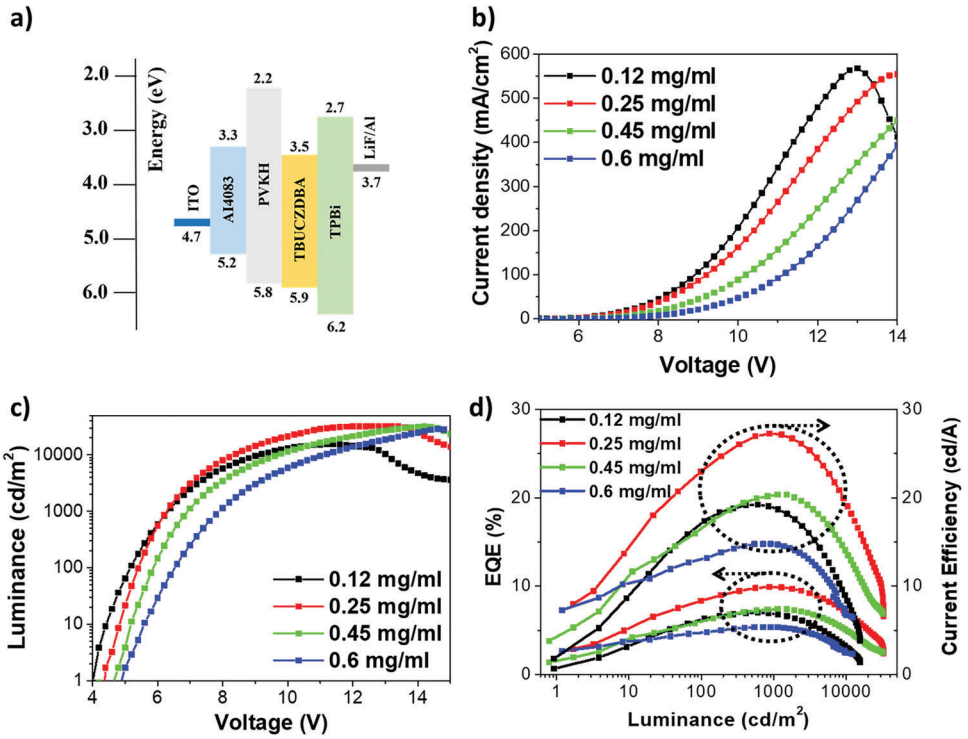

Figure 3. Characterization of OLED device with different thicknesses of inkjet printed tBuCzDBA film as the active layer. a) Device architecture and energy level diagram of the prepared OLEDs; b) current density versus voltage, c) luminance versus voltage, and d) efficiency versus luminance characteristics.

the short decay component in the nanosecond regime can be attributed to prompt fluorescence, while the longer decay components in the microsecond regime can be attributed to TADF.

These characterizations confirm what has already been reported in the literature for this material,[47] and demonstrate the possibility of keeping the optical properties of the material unchanged regardless of the deposition techniques.

2.3. OLED Application

To test the potential of the reported printed thin film as emitting layer in an OLED device, the following stacked architecture was fabricated: ITO (Indium Tin Oxide)/PEDOT:PSS (poly(3,4-ethylenedioxythiophene)polystyrene sulfonate) AI4083/PVK/tBuCzDBA/TPBi (2,2′,2″-(1,3,5-benzinetriyl)-tris(1-phenyl-1-H-benzimidazole))/LiF/Al (**Figure 3**a). Since OLED efficiency can strongly depend on the thickness of the emitting layer, devices with different tBuCzDBA thicknesses were prepared to find the one that maximizes the performance. Therefore, the emitting layer was printed from ink with different concentrations (0.12–0.25–0.45–0.6 mg mL^{-1}) obtaining the following thicknesses: 13±5, 18±3, 27±3, and 47±2 nm. We observed that the tBuCzDBA concentration in the investigated range did not affect the ink printability and the thin film formation. In Figure S1 (Supporting Information), the rheological characterization of the ink at 0.25 mg mL^{-1} is compared with that at 0.6 mg mL^{-1} and the curves are overlapped, thus demonstrating that the inks show the same rheological behavior. Moreover, in Table S1 (Supporting Information) the surface tension values of the four inks are reported and again there are no significant differences. The current density versus voltage (J vs V), luminance versus voltage (L vs V), and efficiency versus luminance (EQE vs L, CE vs L) curves for the best devices with tBuCzDBA as EML are shown in Figure 3b–d, respectively.

As shown in Figure 3b, OLEDs with thinner tBuCzDBA had the highest current densities due to the lower resistance. All the devices had maximum luminance, maximum CE, and maximum EQE higher than 10 000 cd m^{-2}, 14 cd A^{-1}, and 5% respectively, and all performance are summarized in **Table 2**. Moreover, a table with average luminance and efficiency values is reported below (**Table 3**). The average values confirm the trend observed with the best devices.

Among the prepared devices, the best performance was achieved by using a printed layer with a thickness of 18 ± 3 nm, achieving a maximum luminance of 32 000 cd/m^{-2} at 13 V, a maximum CE and maximum EQE of 27.5 cd A^{-1} and 10% respectively. Devices with greater tBuCzDBA thicknesses showed a higher turn-on voltage and lower luminances probably due to charge unbalancing into the device.

As a reference, a device with spin coated tBuCzDBA layer was fabricated and compared with the best-printed device (Figure S7, Supporting Information). We selected a spin-coated device with an active layer of comparable thickness to that of the best inkjet device. As can be seen, the current efficiency of the spin-coated device is about half that of the printed device. We attributed the large difference in efficiency to the redissolution phenomenon mentioned above, combined with the different nature of the deposition technique. Indeed, considering the partial redissolution

Table 2. Summary table of best OLED device performance with inkjet-printed tBuCzDBA.

tBuCzDBA thickness [nm]	Maxim Current Density [mA cm^{-2}]	Turn on voltage [V]	Maximum Luminance [cd m^{-2}]	CE at 100 cd m^{-2} [cd A^{-1}]	CE at 1000 cd m^{-2} [cd A^{-1}]	Maximum CE [cd A^{-1}]	Maximum EQE [%]
13 ± 5	525 @14V	4.4	15 451 @11.2V	17.4	18.8	19.2 [597 cd m^{-2} @6 V]	7.8
18 ± 3	554 @14V	4.8	32 496 @13V	22.96	27.1	27.2 [866 cd m^{-2} @6.2 V]	9.9
27 ± 3	450 @14V	5.2	31 514 @14V	16.5	20.2	20.4 [1127 cd m^{-2} @7 V]	7.4
47 ± 2	393 @14V	5.6	24 878 @14V	11.5	14.7	14.8 [1441 cd m^{-2} @8.2 V]	5.4

of the PVK layer when printing the T#3 ink, in addition to the thinning of the PVK layer, an in situ blend and/or blurred interface may be formed considering the time required for the ink to dry completely. Such a blend/blurred interface could have a significant impact on device performance.

We assume that the PVK-tBuCzDBA mixing does not occur in the spin-coated device, although there is a partial redissolution of the PVK layer. In spin coating, the drying time is much shorter and the excess solvent is quickly removed by centrifugal force, making it easier to form a clear interface between the PVK and the tBuCzDBA. Therefore, a direct comparison between the spin-coated device and the device with the inkjet-printed active layer cannot be made, as the active layers show differences due to the different deposition techniques. In particular, the spin-coated device has a bilayer with a clear interface, whereas the inkjet-printed layer has a blurred interface. To support our hypothesis, we fabricated a spin-coated device that attempted to reproduce the architecture of the printed device, i.e., by thinning the PVK layer thickness and using a PVK:tBuCzDBA blend as the active layer. The performance of such a device is shown in Figure S7 (Supporting Information), and as can be seen, a significant performance improvement is visible, with current efficiencies close to those of the printed device. Such data support our hypothesis regarding the formation of a blend/blurred interface. Moreover, we were able to obtain such a performance improvement by using two single-material layers instead of preparing complex host-guest systems.

In **Table 4**, the performance of our devices was compared to that of other tBuCzDBA-based devices fabricated using different deposition techniques.

While thermal evaporated and spin-coated host-guest systems provided very high performance, this is the first time that tBuCzDBA has been used as a self-hosted printed TADF material and the performance achieved represents the state of the art for this type of printed emitting layer in OLEDs (see Table S2, Supporting Information).

Table 3. OLEDs average luminance and efficiency according to the active layer thickness.

tBuCzDBA thickness [nm]	Maximum Luminance [cd m^{-2}]	Maximum CE [cd A^{-1}]
13 ± 5	13 332 ± 940	18.4 ± 1.2
18 ± 3	30 260 ± 1602	24.5 ± 1.5
27 ± 3	29 502 ± 1480	18.6 ± 1.4
47 ± 2	20 340 ± 2337	11.9 ± 1.7

3. Conclusions

In this paper the ink optimization for printing tBuCzDBA as an emitting layer in OLEDs has been reported. The optimized printed thin film was obtained by using a proper mixture of three solvents (toluene /chloroform/o-dichlorobenzene) with different surface tensions, which induced Marangoni flows in the wet film and allowed a uniform and fast drying process.

Chlorinated solvents and other commonly used solvents for printing techniques can certainly be a problem for the industrial scalability, considering that they are toxic and dangerous to humans and the environment, but they still represent an important reality in the field of industrial processes and the fabrication of optoelectronic devices with organic materials.

The printed tBuCzDBA emissive layer, obtained with the optimized solvents formulation, showed very good morphology and low roughness. The time-resolved photophysical study demonstrates that this film shows TADF properties. The resulting inkjet-printed thin film was employed as an emissive layer in an OLED structure, varying the concentration of tBuCzD in the ink to obtain optimized films thickness and device performance. The device with 18 nm of tBuCzDBA showed a maximum luminance of 32 000 cd m^{-2} at 13 V, a max-CE of 27.5 cd A^{-1}, and an EQE of 10%. The reported results demonstrates that the optimized ink formulation can be considered a powerful tool to easily inkjet print small molecule active layers in OLEDs, achieving excellent morphological, optical, and electro-optical properties. The possibility of using a self-hosted material in the emissive layer of an OLED allows to simplify the design of the device. In addition, solution-based, low-cost, and industrially scalable manufacturing techniques expand the application of OLED technology across multiple sectors at significantly reduced costs.

4. Experimental Section

Chemicals and Reagents: tBuCzDBA was purchased from Lumtec, PEDOT:PSS AI 4083 was purchased from Heraeus Clevios. Poly(9-vinylcarbazole) (PVK, average $M_w \approx 1\,100\,000$, powder) and all other chemicals/solvents were purchased from Sigma-Aldrich. All chemicals were used as received without any further purification.

Ink and Film Characterization: The viscosity of the formulations was evaluated through a strain-controlled rheometer (Ares TA instrument) equipped with parallel plate geometry (diameter = 25 mm). The measurements were performed in steady mode at 20 °C at a shear rate ranging from 10 to 100 s^{-1}.

The CAM 200 (KSV Instruments Ltd., Finland) instrument was used to perform pendant drop measurement, to evaluate the surface tension of

Table 4. Comparative table of OLEDs with tBuCzDBA as emitting material.

Year	Active layer deposition technique	Device structure	Performances	Ref.
2018	Thermal evaporation	ITO/NPB/TCTA/CBP:tBuCzDBA (10%)/TmPyPB/LiF/Al	Maximum luminance of 60 000 cd m^{-2}, EQE of 32.4 ± 1.3% and CE of 127.9 ± 3.1 cd A^{-1}	[47]
2021	Spin coating	ITO/PEDOT: PSS/H2:tBuCzDBA (10%)/B3PyMPM/LiF/Al	Maximum luminance of 10 000 cd m^{-2}, EQE of 26.4% and CE of 85.5 cd A^{-1}	[49]
2022	Thermal evaporation	ITO/TAPC/TCTA/tBuCzDBA/B4PYMPM/LiF/Al	Maximum luminance of 45 727 cd m^{-2}, EQE of 26.9%, and CE of 86.9 cd A^{-1}	[50]
2023	Spin coating	ITO/PEDOT:PSS/2FTAT-1Ph:tBuCzDBA (10%)/TmPyPB/LiF/Al	Maximum luminance of 9879 cd m^{-2}, EQE of 20.9%, and CE of 69.5 cd A^{-1}	[48]
2023	Inkjet printing	ITO/PEDOT:PSS /PVK/tBuCzDBA/TPBi/LiF/Al	Maximum luminance of 32 000 cd m^{-2} at 13 V, a max-CE of 27.5 cd A^{-1}, and an EQE of 10%.	This work
2023	Spin coating	ITO/PEDOT:PSS /PVK/tBuCzDBA/TPBi/LiF/Al	Maximum luminance of 27 000 cd m^{-2} at 12 V, a max-CE of 13.6 cd A^{-1}, and an EQE of 5%.	This work
2023	Spin coating	ITO/PEDOT:PSS /PVK/PVK:tBuCzDBA/TPBi/LiF/Al	Maximum luminance of 19 500 cd m^{-2} at 9 V, a max-CE of 28 cd A^{-1}, and an EQE of 10%.	This work

all solutions. The reported data are the average of three measurements with standard deviations from the medium value. The same CAM 200 apparatus was used to allow static contact angle measurements of all the solutions by the sessile drop method. Several drops of each solution were deposited onto different areas of the glass substrates and observed for 60 s, and then the respective averages and standard deviations were reported. Images of the dried drops were taken using a Dino-Lite digital microscope.

Films thicknesses were measured through a surface profiler (Dektak) characterized by a mechanical stylus with a 12 µm tip diameter. Ink-jet printed films were characterized by a Leica TCS SP5 confocal laser scanning microscope (Leica Microsystem GmbH, Mannheim, Germany) using a 20x dry obiective and by Atomic Force Microscopy (Nanosurf EasyScan 2) in the non-contact mode using silicon tips with a nominal tip radius being less than 10 nm and WS × M was used for the image analysis.

Fluorescence spectroscopic studies were performed with an Edinburgh FLS980 spectrometer equipped with a Peltier-cooled Hamamatsu R928 photomultiplier tube (185–850 nm), at 25 °C. Corrected spectra were obtained via a calibration curve supplied with the instrument. For the emission spectra, the widths of the slits were adjusted between 1 and 5 nm, integration time = 0.1 s, 1 nm step. For all solid films, PLQYs have been calculated by corrected emission spectra obtained from an apparatus consisting of a barium sulphate-coated integrating sphere (4 or 6 inches), a 450 W Xe lamp (λ_{exc} = tunable by a monochromator supplied with the instrument) as light sources, and an R928 photomultiplier tube as signal detectors, following the procedure described by De Mello et al.[54]

Emission lifetimes in the ns-µs range were determined, by the time-correlated single-photon counting (TCSPC) technique by means of the same Edinburgh FLS980 spectrometer using a laser diode as excitation source (EPL 1 MHz, λ_{exc} = 400 nm) and an Peltier-cooled Hamamatsu tube R928 photomultiplier tube as detector. Analysis of the luminescence decay profiles versus time was accomplished with the DAS6 Decay Analysis Software provided by the manufacturer. The quality of the fit was estimated by visual inspection of the weighted residuals and calculation of χ^2.

Experimental uncertainties are estimated to be ± 8% for lifetime determinations, ± 10% for emission quantum yields, ± 5 nm for absorption and emission peaks.

OLEDs Fabrication and Characterization: The structure of fabricated OLEDs with inkjet-printed active layer consists of Glass/ITO/PEDOT:PSS AI4083/PVK/tBuCzDBA/TPBi/LiF/Al. The glass/ITO substrates were cleaned with acetone and isopropyl alcohol for 10 min each and dried with nitrogen. PEDOT:PSS (Clevios AI4083) and PVK (high molecular weight M_w ≈1.100.000) were used as hole injection layer and hole transport layer, respectively. PEDOT:PSS AI4083 was deposited through spin coating. Before the spin coating, a plasma oxygen treatment was performed on the glass/ITO substrates (50 W, O_2 flow 30 sccm). PEDOT:PSS AI4083 solution without any modification was spin-coated at 3000 rpm for 30 sec and then annealed at 120 °C for 15 min. PVK 5 mg mL^{-1} in chlorobenzene/chloroform 5/95 volume ratio was then spin-coated at 7000 rpm for 40 sec and annealed at 110 °C for 5 min. tBuCzDBA layers were printed using a custom-made inkjet printer fabricated by T.P.A. s.r.l. and provided with a single nozzle with a diameter of 300 um. The single nozzle printer moves at 1 m min^{-1} on the fixed glass substrate, it ejects drops with a volume of ≈15 nL from a height of 7 mm above the substrate. The individual circular drops are separated by a distance of 1 mm (center to center). The final printed layers have dimensions of ≈3 cm^2. The printed tBuCzDBA layers were dried for 1 min at room temperature and then annealed at 110 °C for 5 min. Subsequently, 50 nm TPBi, 0.8 nm LiF, and 100 nm Al were deposited by vacuum thermal evaporation in a Kurt J. Lesker multiple high-vacuum chamber system. The effective light-emitting area of fabricated devices is 15 mm^2.

The reference spin coated device has the following structure: glass/ITO/PEDOT:PSS AI4083/PVK/tBuCzDBA/TPBi/LiF/Al, in which tBuCzDBA was spin-coated (2000 rpm x 60 sec) starting from a toluene solution (10 mg mL^{-1}).

The reference spin coated device with a blend as active layer has the following structure: glass/ITO/PEDOT:PSS AI4083/PVK/PVK:tBuCzDBA/TPBi/LiF/Al. The PVK was spin-coated starting from a 3 mg mL^{-1} in chlorobenzene/chloroform 5/95 volume ratio solution (7000 rpm x 40 sec), while the active layer was spin coated (2000 rpm x 60 sec) starting from a toluene solution (10 mg mL^{-1}) with a PVK:tBuCzDBA ratio of 30:70.

The optoelectronic characteristics of the OLED devices were measured in a glove box using an Optronics OL770 spectrometer coupled to the OL610 telescope unit with an optical fiber for the luminance measurements. The whole system was directly connected by an RS232 cable to a Keithley 2420 current–voltage source meter. The average device performance in terms of luminance and efficiency was calculated from the characterisations of a statistical sample consisting of 12 devices with the same structure.

Supporting Information

Supporting Information is available from the Wiley Online Library or from the author.

Acknowledgements

M.C. and C.T.P. contributed equally to this work. The authors thank Iolena Tarantini, Sonia Carallo, Antonio Andretta, Daniele Greco, Roberto

Giannantonio for their technical and scientific support. This work was supported by: "ECO-sustainable and intelligent fibers and fabrics for TEChnic clothing (ECOTEC)", PON «R&I» 2014–2020, project N° ARS01_00951, CUP B66C18000300005; "Tecnopolo per la medicina di precisione" (Tecnomed Puglia)-Regione Puglia: DGR n. 2117 del 21/11/2018, CUP: B84I18000540002; PE4 PNRR MUR project PE0000023–NQSTI; PNRR MUR project IR0000016–I–PHOQS; the Italian Ministry of Research (MUR) under the complementary actions to the NRRP (PNC0000007) "Fit4MedRob- Fit for Medical Robotics" Grant (contract number CUP B53C22006960001).

Conflict of Interest

The authors declare no conflict of interest.

Data Availability Statement

The data that support the findings of this study are available from the corresponding author upon reasonable request.

Keywords

inkjet printing, OLEDs, self-hosted, solution processed, TADF

Received: May 31, 2023
Revised: August 22, 2023
Published online:

[1] R. H. Friend, R. W. Gymer, A. B. Holmes, J. H. Burroughes, R. N. Marks, C. Taliani, D. D. C. Bradley, D. A. D. Santos, J. L. Brédas, M. Lögdlund, W. R. Salaneck, *Nature* **1999**, *397*, 121.
[2] P. Y. Chen, C. C. Chen, C. C. Hsieh, J. M. Lin, Y. S. Lin, Y. Lin, in *Dig. Tech. Pap. – SID Int. Symp.*, **2015**, pp. 1352–1354.
[3] Y. Kajiyama, K. Kajiyama, H. Aziz, *Opt. Express* **2015**, *23*, 16650.
[4] N. Sain, *Int. J. Eng. Appl. Sci. Technol.* **2020**, *4*, 587.
[5] A. M. Bagher, *Int. J. Adv. Res. Phys. Sci.* **2017**, *4*, 48.
[6] A. Salehi, X. Fu, D.-H. Shin, F. So, *Adv. Funct. Mater.* **2019**, *29*, 1808803.
[7] S.-J. Zou, Y. Shen, F.-M. Xie, J.-D. Chen, Y.-Q. Li, J.-X. Tang, *Mater. Chem. Front.* **2020**, *4*, 788.
[8] D. Ma, C. Zhang, R. Liu, Y. Qiu, L. Duan, *Chem. – A Eur. J.* **2018**, *24*, 5574.
[9] H. Gorter, M. J. J. Coenen, M. W. L. Slaats, M. Ren, W. Lu, C. J. Kuijpers, W. A. Groen, *Thin Solid Films* **2013**, *532*, 11.
[10] D. Ma, C. Zhang, Y. Qiu, L. Duan, *Chem. – A Eur. J.* **2016**, *22*, 15888.
[11] J. Eccher, W. Zajaczkowski, G. C. Faria, H. Bock, H. Von Seggern, W. Pisula, I. H. Bechtold, *ACS Appl. Mater. Interfaces* **2015**, *7*, 16374.
[12] S. Burns, J. Macleod, T. Trang Do, P. Sonar, S. D. Yambem, *Sci. Rep.* **2017**, *7*, 40805.
[13] H. A. Méndez-Pinzón, D. R. Pardo-Pardo, J. P. Cuéllar-Alvarado, J. C. Salcedo-Reyes, R. Vera, B. A. Páez-Sierra, *Univ. Sci.* **2010**, *15*, 68.
[14] Y. Chen, J. Wang, Z. Zhong, Z. Jiang, C. Song, Z. Hu, J. Peng, J. Wang, Y. Cao, *Org. Electron.* **2016**, *37*, 458.
[15] Q.-S. Tian, W.-S. Shen, Y.-J. Yu, X.-Q. Wang, J.-H. Cai, Y. Hu, Z.-Q. Jiang, J.-S. Huang, L.-S. Liao, *Org. Electron.* **2022**, *100*, 106366.
[16] T. J. Routledge, D. G. Lidzey, A. R. Buckley, *AIP Adv.* **2019**, *9*, 15330.
[17] N. Sahu, B. Parija, S. Panigrahi, *Indian J. Phys.* **2009**, *83*, 493.
[18] L. E. Scriven, *MRS Online Proc. Libr* **1988**, *121*, 717.
[19] Y. Xiao, C. Zuo, J.-X. Zhong, W.-Q. Wu, L. Shen, L. Ding, *Adv. Energy Mater.* **2021**, *11*, 2100378.
[20] S. Magdassi, **2009**, 356.
[21] R. Tortorich, J.-W. Choi, *Nanomaterials* **2013**, *3*, 453.
[22] M. Singh, H. M. Haverinen, P. Dhagat, G. E. Jabbour, *Adv. Mater.* **2010**, *22*, 673.
[23] M. Montanino, G. Sico, C. T. Prontera, A. De Girolamo Del Mauro, S. Aprano, M. G. Maglione, C. Minarini, *eXPRESS Polym. Lett.* **2017**, *11*, 518.
[24] B.-J. De Gans, P. C. Duineveld, U. S. Schubert, *Adv. Mater.* **2004**, *16*, 203.
[25] M. Singh, H. M. Haverinen, P. Dhagat, G. E. Jabbour, *Adv. Mater.* **2010**, *22*, 673.
[26] L. Zhou, L. Yang, M. Yu, Y. Jiang, C.-F. Liu, W.-Y. Lai, W. Huang, *ACS appllied Mater. interfaces* **2017**, *9*, 40533.
[27] D. Li, W. Lai, Y. Zhang, W. Huang, *Adv. Mater.* **2018**, *30*, 1189.
[28] X. Peng, J. Yuan, S. Shen, M. Gao, A. S. R. Chesman, H. Yin, J. Cheng, Q. Zhang, D. Angmo, *Adv. Funct. Mater.* **2017**, *27*, 1703704.
[29] E. Menard, M. A. Meitl, Y. Sun, J.-U. Park, D. J.-L. Shir, Y.-S. Nam, S. Jeon, J. A. Rogers, *Chem. Rev.* **2007**, *107*, 1117.
[30] M. Fang, J. Yang, Z. Li, *Prog. Mater. Sci.* **2022**, *125*, 100914.
[31] Y. Liu, G. Xie, K. Wu, Z. Luo, T. Zhou, X. Zeng, J. Yu, S. Gong, C. Yang, *J. Mater. Chem. C* **2016**, *4*, 4402.
[32] Y. Suzuki, Q. Zhang, C. Adachi, *J. Mater. Chem. C* **2015**, *3*, 1700.
[33] Y. J. Cho, B. D. Chin, S. K. Jeon, J. Y. Lee, *Adv. Funct. Mater.* **2015**, *25*, 6786.
[34] A. Maggiore, X. Tan, A. Brosseau, A. Danos, F. Miomandre, A. P. Monkman, P. Audebert, G. Clavier, *Phys. Chem. Chem. Phys.* **2022**, *24*, 17770.
[35] A. Maggiore, Y. Qu, R. Guillot, P. Pander, M. Vasylieva, P. Data, F. B. Dias, P. Audebert, G. Clavier, F. Miomandre, *J. Phys. Chem. B* **2022**, *126*, 2740.
[36] Y. Xie, Z. Li, *J. Polym. Sci. Part A Polym. Chem.* **2017**, *55*, 575.
[37] G. Xie, J. Luo, M. Huang, T. Chen, K. Wu, S. Gong, C. Yang, *Adv. Mater.* **2017**, *29*, 1604223.
[38] J. Luo, G. Xie, S. Gong, T. Chen, C. Yang, *Chem. Commun.* **2016**, *52*, 2292.
[39] S. Y. Lee, T. Yasuda, H. Komiyama, J. Lee, C. Adachi, *Adv. Mater.* **2016**, *28*, 4019.
[40] K. Matsuoka, K. Albrecht, A. Nakayama, K. Yamamoto, K. Fujita, *ACS Appl. Mater. Interfaces* **2018**, *10*, 33343.
[41] K. Albrecht, K. Matsuoka, K. Fujita, K. Yamamoto, *Mater. Chem. Front.* **2018**, *2*, 1097.
[42] K. Albrecht, K. Matsuoka, K. Fujita, K. Yamamoto, *Angew. Chemie – Int. Ed.* **2015**, *54*, 5677.
[43] Z. Yang, Z. Mao, Z. Xie, Y. Zhang, S. Liu, J. Zhao, J. Xu, Z. Chi, M. P. Aldred, *Chem. Soc. Rev.* **2017**, *46*, 915.
[44] M. K. Etherington, J. Gibson, H. F. Higginbotham, T. J. Penfold, A. P. Monkman, *Nat. Commun.* **2016**, *7*, 13680.
[45] C. Amruth, B. Luszczynska, M. Zdzislaw, J. Ulanski, K. Albrecht, K. Yamamoto, *Org. Electron.* **2019**, *74*, 218.
[46] C. M. Cole, S. V. Kunz, P. E. Shaw, C. S. K. Ranasinghe, T. Baumann, J. P. Blinco, P. Sonar, C. Barner-Kowollik, S. D. Yambem, *Adv. Mater. Technol.* **2022**, *7*, 2200648.
[47] T.-L. Wu, M.-J. Huang, C.-C. Lin, P.-Y. Huang, T.-Y. Chou, R.-W. Chen-Cheng, H.-W. Lin, R.-S. Liu, C.-H. Cheng, *Nat. Photonics* **2018**, *12*, 235.
[48] Y. Liu, Y. Wu, T. Wang, Q. Wang, X. Han, X. Wu, H. Tong, L. Wang, *Org. Electron.* **2023**, *113*, 106720.
[49] L. Chen, J. Lv, S. Wang, S. Shao, L. Wang, *Adv. Opt. Mater.* **2021**, *9*, 2100752.

[50] T.-L. Wu, J. Lei, C.-M. Hsieh, Y.-K. Chen, P.-Y. Huang, P.-T. Lai, T.-Y. Chou, W.-C. Lin, W. Chen, C.-H. Yu, L.-Y. Hsu, H.-W. Lin, C.-H. Cheng, *Chem. Sci.* **2022**, *13*, 12996.
[51] C. Seo, D. Jang, J. Chae, S. Shin, *Sci. Rep.* **2017**, *7*, 500.
[52] M. Cinquino, C. T. Prontera, A. Zizzari, A. Giuri, M. Pugliese, R. Giannuzzi, A. G. Monteduro, M. Carugati, A. Banfi, S. Carallo, A. Rizzo, A. Andretta, G. Dugnani, G. Gigli, V. Maiorano, *J. Sci. Adv. Mater. Devices* **2021**, 100394.
[53] A. D. Nikolov, D. T. Wasan, P. Wu, *Curr. Opin. Colloid Interface Sci.* **2021**, *51*, 101387.
[54] J. C. De Mello, H. F. Wittmann, R. H. Friend, *Adv. Mater.* **1997**, *9*, 230.